# Black Lipid Membranes: Visualizing the Structure, Dynamics, and Substrate Dependence of Membranes

**Ryan S. Ries,[†] Hyeon Choi,[†] Rikard Blunck,[‡] Francisco Bezanilla,[‡,§] and James R. Heath*[,†]**

*Department of Chemistry, Division of Chemistry and Chemical Engineering, MC 127-72, The California Institute of Technology, Pasadena, California 91125, and The Departments of Physiology and Anesthesiology, David Geffen School of Medicine at the University of California, Los Angeles, California 90095*

*Received: May 3, 2004*

The structure and long-time dynamics of suspended lipid bilayers made of 1-stearoyl-2-oleoyl-*sn*-glycero-3-phosphoethanolamine (SOPE) in the gel phase was interrogated using electrical measurements co-recorded with second harmonic generation (SHG) micrographs. SHG microscopy was shown to be an efficient method for distinguishing between the regions of bilayer and annulus as well as probing structural and dynamical variations within a single bilayer. Micromachined silicon chips and two types of plastic partitions, delrin and polyethylene, were investigated as substrate materials. Silicon chips yielded the most stable bilayers, lasting for 1 or 2 days. The membrane characteristics, including the amount of incorporated solvent within the bilayer, the dynamics of bilayer formation, and the stability of the bilayer, were found to be strongly substrate-dependent. In a second set of experiments, SHG-active membrane dyes, di-8-ANEPPS and di-4-ANEPPS, were used to interrogate the domain structure of the same suspended bilayers using scanning two-photon fluorescence (2PF) and SHG microscopy, again correlated with capacitance measurements. Using these dyes, an enhancement in the SHG signal due to membrane potential was recorded, and the rates of molecular diffusion for di-4-ANEPPS through the membrane were investigated. Polarization-resolved SHG imaging was used to determine the orientation of the dye molecules within the membrane.

## 1. Introduction

**1.1. Lipid Bilayers.** Lipid bilayers are central components of cellular membranes, playing important roles in mass transport in and out of cells, cell structure, protein host matrixes, energy generation and storage, and so forth. Many different model systems have been developed to elucidate the properties of lipid bilayers that are free from interactions with other cellular machinery.[1−5] These model membranes range from giant unilamellar vesicles to planar supported and suspended lipid bilayers. One of the most useful systems is the classic black lipid membrane (BLM) first described by Mueller.[6] This model system is a reasonably close semblance of an actual cell membrane because it permits simultaneous access to the solution and electrical control of both sides of the bilayer, allowing for the mimicking of physiological conditions. For example, a number of researchers have investigated BLMs as host matrixes for membrane proteins.

BLMs are known to consist of three components: lipid bilayers, a thicker annulus that forms at the interface between the supporting substrate and the bilayer, and microlenses (pockets of decane). Cell membranes are a fluid system that temporally evolves according to the phase behavior of the lipids.[7,8] In bilayer systems, the annulus, microlenses, and bilayer regions can all participate in this evolution. However, the characterization of the static and dynamic structure of BLMs has been hampered by the lack of suitable optical techniques.[2,9,10] Because lipid bilayers are only a few nanometers thick, optical images of BLMs tend to appear black or gray, although fluorescent probe molecules have been utilized to track phenomena such as lateral molecular diffusion within the bilayer.[11−14] In addition, every painted BLM is unique, depending not only on the lipids and supporting material but also on the phenomenology of the process used to create the bilayer; consequently, even simple observables such as the membrane capacitance are not always straightforward to interpret because of changes in the bilayer area and solvent content within the bilayer.

Membranes exhibit significant structural variations across different preparation procedures. Some of these differences can be normalized against by using the parameter of specific capacitance ($C_m$), or capacitance per unit bilayer area. Most reports on the electrical properties of BLMs have investigated $C_m$ values immediately following the formation of the bilayer and then for a short time (an hour or less) afterward. Values of $C_m$ vary widely, but limits have been established. Large $C_m$ values correspond to compressed bilayers with no solvent (decane, for example) between the phospholipid tails, and the highest value of $C_m$ reported is 1.5 $\mu$F/cm$^2$, although most researchers use an upper limit of 1.0 $\mu$F/cm$^2$. The lower limit is 0.3 $\mu$F/cm$^2$, and values in this range correspond to bilayers that are highly expanded, likely containing organic solvent between the phospholipid tails.[2,15,16] Measured $C_m$ values, as well as the stability of the bilayers, exhibit a dependence upon the suspending substrate material.

Here we report on two sets of experiments designed to quantify the structure, dynamics, and electrical properties of suspended BLMs. In section 3, we employ a coherent (polariza-

* Corresponding author. E-mail: heath@caltech.edu.
[†] The California Institute of Technology.
[‡] The Department of Physiology, David Geffen School of Medicine at the University of California.
[§] The Department of Anesthesiology, David Geffen School of Medicine at the University of California.

10.1021/jp048098h CCC: $27.50 
Published on Web 07/02/2004

tion-resolved second harmonic generation (SHG)) (two photon) imaging technique, coupled with capacitance measurements, for BLMs suspended across three types of supporting substrates: micromachined silicon wafers and two types of plastic partitions, delrin and polyethylene. We first report on the suitability of SHG microscopy for probing the BLM structures. We then present time-dependent nonlinear optical and electrical measurements, which allowed us to record and quantify the dynamics of bilayer formation and evolution.

We interrogate BLMs at the molecular level by quantifying the interaction of particular dye molecules with the lipid matrix in section 4. We employed both polarization-resolved SHG and two-photon fluorescence (2PF) imaging techniques, both simultaneously collected and recorded with capacitance measurements, for BLMs suspended across the same three substrates. We utilized the dye molecules di-4-ANEPPS and di-8-ANEPPS as structural probes of BLMs. Both dyes possess an electric-field-dependent second-order nonlinear susceptibility ($\chi^{(2)}$) but have different chemical interactions with the bilayers. Di-4-ANEPPS will undergo flip-flop through the membrane, meaning that it will diffuse from one side of the bilayer to the other. Conversely, di-8-ANEPPS, with its longer acyl chain, does not flip-flop and so is a stable probe for interrogating the long-time dynamics of bilayer domain structures. We quantify the rates of molecular diffusion through the membrane as well as the structure and dynamics of dye-containing bilayer domains. Finally, polarization-dependent SHG imaging was utilized to interrogate the molecular orientation of the dye molecules when they were partitioned into the BLMs.

**1.2. SHG Imaging of BLMs: Background.** Suspended lipid bilayers can be thought of as a three-phase material consisting of a hydrocarbon phase sandwiched between two aqueous phases. Interface-rich systems are often uniquely interrogated using second-harmonic generation (SHG) and sum-frequency generation spectroscopy. We employed SHG microscopy, correlated with electrical measurements, to characterize BLMs.

SHG is a coherent scattering phenomenon that does not require fluorophores but does require a broken-symmetry interface and, as we discuss here, can allow for the visualization of certain regions of a suspended bilayer. A fully symmetric bilayer would not generate significant SHG signal unless the two oppositely oriented monolayers of amphiphile were separated by a distance that was greater than the coherence length for SHG, which is typically around 2 $\mu$m for bilayer systems,[17] or if there was some domain structure that was asymmetric across the bilayer, such as microlenses. In the idealized drawing of the suspended bilayer presented in Figure 1, the central portion of the bilayer should clearly not generate SHG signal because there is no broken interface symmetry and the bilayer is only approximately 5 nm thick, a dimension that is small compared to the coherence length. The outer region is referred to as the annulus and is composed of a mixture of organic solvent and lipids. In the annulus, the interface symmetry is broken because of the decane between the lipid tails, so this region should generate the largest SHG signal.

A perfect bilayer would be highly symmetric and so not expected to generate SHG signal. However, a more realistic approximation for a gel-phase bilayer is that there may are domains of reduced symmetry, such as microlenses, that can generate finite (albeit weak) SHG signal. The SHG micrograph in Figure 1A (collected from one of our silicon partitions) reveals this type of signal—no SHG within the region of the thin bilayer but measurable signal within the region of the thicker annulus. The annulus is not uniform, apparently, so the

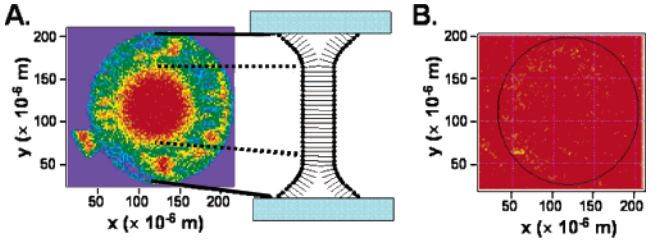


**Figure 1.** (A) SHG image of a bilayer suspended across a pore (through a silicon substrate). The image was collected using polarization-resolved SHG microscopy. The image reveals two regions—a central (red) area that yields no SHG signal and a perimeter region that apparently has some structure. An idealized drawing of the bilayer is represented at the right of the image. The central region represents a thin, symmetric bilayer in which the hydrophobic tails of the phospholipids have squeezed out any organic solvent. The annulus region lacks the symmetry of the central region and can yield a finite SHG signal. (B) Two-photon-fluorescence image, collected with a filter in place to remove any SHG, reveals no fluorescence from the bilayer.

SHG signal arising from that region exhibits some structure. A two-photon fluorescence (2PF) image collected from the same bilayer (Figure 1B) yields no signal because no fluorescing molecules were incorporated into the bilayer. The experimental details of how these images were collected are presented below. Related instruments have been used to look at giant unilamellar vesicles in solution.[18] There have been several other studies using both polarization-resolved and nonpolarization-resolved SHG to image cells and hemispherical lipid bilayers[19−23] along with numerous studies using 2PF microscopy.[24,25]

## 2. Materials and Methods

**2.1. Substrates.** Three different types of materials—silicon wafers (Virginia Wafernet), polyethylene (McMaster Carr), and delrin (McMaster Carr)—were used to make supports for the suspended bilayers. Two different techniques to make pores and fluid channels in the substrates were developed. Polyethylene and delrin substrates were machined using standard machining tools, and the silicon was micromachined in a semiconductor fabrication facility

For polyethylene and delrin substrates, the material was washed thoroughly in an Alconox powder detergent solution followed by an ethanol rinse. An aluminum mold was machined with 1-mm-wide straight lines, for molding fluid channels, and was clamped into the material, and the assembly was baked in an oven (80 °C for polyethylene; 140 °C for delrin) for approximately 20 min. More pressure was applied to the mold, and it was placed back into the oven. This was repeated until the channels were pressed almost all the way through the material, leaving an approximately 40-$\mu$m-thick region in the middle of the substrate (Figure 2a). The material was cooled, and a 150-$\mu$m drill bit was used to drill small holes through the substrate channels. The substrates were then sonicated in a detergent solution (Alconox) for 30 min to clean the hole of debris. The drill bit was then heated and inserted into the hole to smooth rough edges. The substrates were sonicated in detergent for 30 min more, sonicated for 20 min in 18 MΩ Millipore water, and then finally rinsed in ethanol and blown dry. This technique facilitates the creation of substrates with uniform hole sizes, shapes, and thickness.

The micromachining of the silicon chips has been reported elsewhere.[26] In short, the chips were microfabricated to have 200-$\mu$m pores in a region that was thinned to be about 40 $\mu$m thick. A 1-$\mu$m-thick $SiO_2$ film was grown over the entire wafer to electrically insulate the front and back sides of the wafer

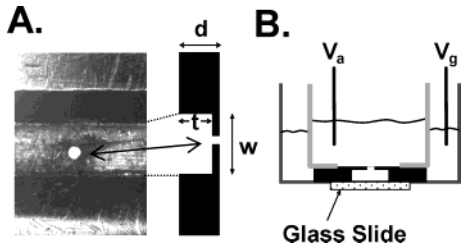


**Figure 2.** (A) Optical micrograph of the delrin substrate. The design of this substrate is the same for polyethylene and is similar to that of the silicon chips. $d = 200$ $\mu$m, $t$ (the depth of the fluid channel) = 150−170 $\mu$m, and $w = 1-2$ mm. (B) Schematic of the assembled bilayer chamber for optical investigations. $V_a$ = applied voltage and $V_g$ = ground.

from each other. The $SiO_2$ also adds a smooth edge to the etched pore to facilitate bilayer formation. A final silanization step was performed by placing the silicon chips into a custom chip holder and dropping in 100 $\mu$L of tri-*n*-butylchlorosilane (Pfaltz & Bauer) and placing the holder into the oven at 160° C for 24 h. This makes the wafer hydrophobic, which facilitates bilayer formation.

**2.2. Lipid Bilayers.** A single type of phospholipid was used in this study: 1-stearoyl-2-oleoyl-*sn*-glycero-3-phosphoethanolamine (SOPE) from Avanti Polar Lipids. The lipids were stored in chloroform at −78 °C. Prior to use, fresh lipids were dried under nitrogen gas and then dissolved in decane (99+% pure from Sigma Aldrich) to a concentration of 25 mg/mL. The substrates were sealed inside a polycarbonate holder using vacuum grease. This holder consisted of two interlocking cylinders, as seen in Figure 2b. The inner cylinder makes an upper chamber, and the outer cylinder, a lower chamber, enabling electrical and solution control of both sides of the membrane. A glass coverslip was attached to the bottom of the outer cylinder for optical access. For most experiments, the top and the bottom buffer solution consisted of 150 mM KCl and 5 mM KMOPS at a pH of 7.4, although these values (composition and pH) were occasionally varied. A small glass rod was used to paint the bilayers across the holes in the substrates, and optical microscopy was used to verify that no bubble was formed over the pore. A classical electrophysiology patch clamp setup (Dagan 3900A with 3910 expander) was used either to control the voltage across the bilayer or to measure the capacitance of the bilayer. Prior to fabricating the hole, we measured each type of substrate for its intrinsic capacitance. The silicon chip had an intrinsic value of 30 pF, and the delrin and polyethylene had an intrinsic value of 11 pF.

**2.3. Scanning Nonlinear Optical Microscopy.** The suspended lipid bilayers were created in a specially designed sample holder that could be placed in our custom-built scanning nonlinear optical microscope, diagrammed in Figure 3.[27] A broadband femtosecond laser system, operating at 82 MHz (Spectra Physics Tsunami), was the illumination source, with excitation coverage from 720 to 980 nm. The average incident laser power was controlled by a series of neutral density filters. The beam passes through a half-wave plate and a polarizer and is then focused onto the sample at a 45° angle to a spot size of about 1.5-$\mu$m diameter using an aspheric molded gel lens (Thorlab 350170, $f = 6.16$ mm, 0.30 NA). A long-pass filter was placed right before the input lens to block the SHG or fluorescence signals generated in the light passage. A second lens collimated the reflected light. The fundamental wavelength was removed with a short-pass filter, and the SHG and 2PF (450−650 nm) signals were separated using a dichroic mirror (440 nm). Additional band-pass filters (370−430 nm for SHG)

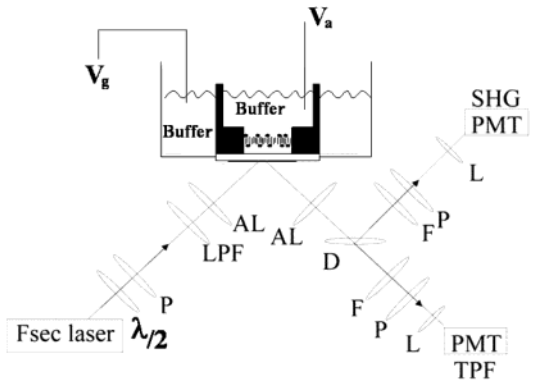


**Figure 3.** Schematic diagram of the scanning nonlinear optical microscope utilized in this study. Abbreviations are as follows: $\lambda/2$ = half-wave plate, P = polarizer, LPF = long-wave pass filter, AL = aspheric lens, L = lens, D = dichroic mirror, and F = filter.

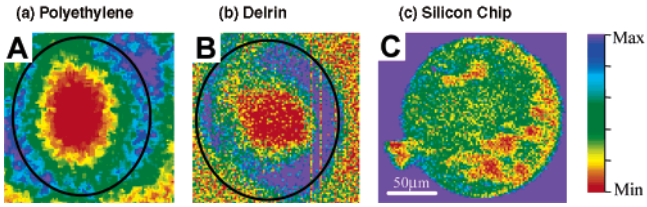


**Figure 4.** SHG images of suspended films (no dye present) on (A) polyethylene, (B) delrin, and (C) a silicon chip. The pore boundaries are shown as solid lines in A and B. In A and B, there is a factor of 40 difference in intensity between green and red, whereas in C, the difference is only a factor of 2.

were installed in front of the SHG detector to ensure that only the signals from the desired spectral regions were recorded. The SHG signal was recorded using photomultiplier tubes attached to preamplifiers and then finally fed into digital lock-in amplifiers, which were synchronized with the chopped laser light at 2 kHz. The direction of the input polarization was manipulated by rotating the half-wave plate and polarizer. The output polarization was selected using a sheet polarizer inserted in front of the detector. The sample was mounted onto a pair of Burleigh inchworm piezoelectric stages, scanning in the $X$ and $Y$ directions.

In these experiments, the laser was set at either 800 or 850 nm with a power of 600 mW. A variety of neutral density filters were then used to interrogate the bilayers. The majority of the time only 5% of the laser intensity was used during the experiments. The time it takes to scan the bilayer was 23 min when using a pixel dwell time of 10 ms. Several different laser powers and dwell times were used, and photodamage never occurred even when using 100% laser power.

## 3. Nonlinear Optical Imaging of BLMs with No Incorporated Dye

**3.1. Bilayers Suspended in Different Materials.** Representative SHG images of suspended films in the three substrate types are shown in Figure 4. In Figure 4a and b, the boundaries of the pores are shown with a black solid line. The boundary of the bilayer is not clear in these images because of the minimal SHG signal arising from the substrates, but it is readily determined when no bilayer has been painted.. The boundary of the hole in a silicon chip is clearly visible in Figure 4c; here, the substrate generates a higher SHG intensity than the suspended film inside the pore. The small notch in the silicon chip is just a defect that occurred during the processing. Note that the pore sizes of polyethylene (150-$\mu$m diameter) and delrin

(150-$\mu$m diameter) were not identical to that of the Si chip (200-$\mu$m diameter) because of the available drill bits. The influence that pore size has on bilayers was studied previously by us using Si chips,[26] and we found that bilayers painted in 150- and 200-$\mu$m pores show similar stability. Pore size mainly affects the capacitance and area of the bilayer, but $C_m$ values for both pore sizes were similar. In our nonlinear optical microscope, the sample is irradiated at 45° so that the entire pore area in a Si chip is not viewable because silicon is not optically clear at 800 nm. Delrin and polyethylene are both optically clear materials, so the entire pore is viewable although there is signal at the pore edges that is caused by the roughening of the plastic surface during the processing. This scatter leads to the moderate signal levels seen around the black circles in Figure 4a and b.

In these studies, we are using a BLM composed of SOPE lipids, which allow for the formation of suspended, single-component bilayers. The particular SOPE lipids used here are in the gel phase at 25 °C. The gel phase is characterized by a highly ordered bilayer structure and yet is still fluid enough to undergo time-dependent structural changes. This makes these SOPE lipids ideal systems for coupling with SHG imaging as a probe of both bilayer structure and dynamics.

In Figure 4a and b, there is a red elliptical region (low SHG signal) in the middle of the hole that is surrounded by an area of higher SHG signal extending to the boundary of the pore. There is a 40-fold difference in the signal intensity between the red and green regions, and this allows us to assign these regions tentatively as the two principal components of the BLM—the central bilayer (red) and the annulus (green and blue). The annulus, which is thicker and less symmetric than the bilayer, should (and does) generate a larger SHG signal. In Figure 4c, the lipid films on the Si chip show a relatively uniform structure without any clear evidence of an annulus. There is only a 2-fold difference between the red and green intensities for these films. The annulus region is hidden in these chips by the boundaries of the pore, indicating that the annulus is quite small. Therefore, the whole (imaged) area of the SOPE film in Figure 4c is tentatively assigned as a bilayer, an assignment that is consistent with the measured $C_m$ values as discussed below.

The BLMs painted on all of the substrates in Figure 4 had $C_m$ values between 0.3 and 1.0 $\mu$F/cm$^2$, indicating that bilayers dominate these films, although the bilayers have different structures depending on the substrate. The bilayer-to-annulus ratio on Si substrates was consistently the largest, but they were also relatively thicker (as measured by the $C_m$ values), possibly containing some decane solvent.

On the basis of this tentative assignment, the size of the annulus region strongly depends on the substrate−lipid interactions. The silanized silicon chips are more hydrophobic, with a contact angle of 102°, in contrast to those of polyethylene (66°) and delrin (60°). The hydrophobic Si chip should stabilize the bilayer more efficiently than the polyethylene and delrin chips, leading to a significantly smaller annulus region. This enhanced stability was consistent with the observation that lipid films formed using the silicon substrates were stable often for a day or two, whereas typical bilayer stability times for polyethylene (4 h) and delrin (2 h) supports were short. Another factor in the bilayer stability was that the chip fabrication process allowed us to form silicon pores that were smoother than the plastic partitions. The substrate dependence of lipid films in plastic and Teflon partitions has been observed previously, using varying substrates and chemical pretreatments of the substrate.[2]

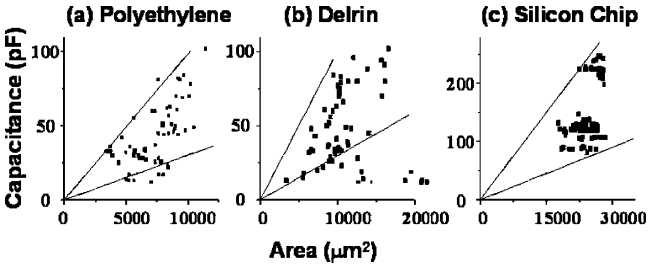


**Figure 5.** Capacitance vs area in (a) polyethylene, (b) delrin, and (c) a silicon chip with the lower (0.3 $\mu$F/cm$^2$) and upper (1.0 $\mu$F/cm$^2$) limits of literature values shown by the lines. Within these limits, one expects a bilayer to be present, and below the limits, a multilayer. Each image shows data from 10 bilayers with the average number of measurements per bilayer of 6 or 7 for the plastic partitions and 10 for the silicon chips.

**3.2. Proof of Bilayer Formation.** Two alternative methods were correlated with the microscopy techniques to verify that the tentatively assigned bilayer regions were true bilayers rather than multilayers, liposomes, or some other metastable state of the lipids. The first was measurements of gramicidin channel activity, and the second was measurements of the BLM capacitance.

*3.2.1. Qualitative Measurement (Gramicidin Channel Activity).* The bacterial channel gramicidin constitutes a qualitative probe of lipid bilayers because it can form a conducting dimer only when two monomer moieties, situated on either side of the membrane, combine. When the gramicidin was reconstituted into the bilayer using all three substrate types, single-channel activity was recorded. The experiment was conducted using a 1 M NaCl solution on the bottom side and a 100 mM NaCl solution on the top side of the bilayer. A 5 $\mu$g/mL solution of gramicidin was prepared, and then 2 $\mu$L of the solution was added to the top solution; after 5 min, single-ion-channel recordings were taken. Single ion channels were detected in bilayers with capacitances as low as 20 pF in polyethylene, 25 pF in delrin, and 90 pF in silicon chips.

*3.2.2. Quantitative Measurement (Specific Capacitance of a Bilayer).* The second method to verify the presence of a true bilayer is a comparison of the $C_m$ values of lipid films in our experiment with literature values. Full area images of suspended bilayers with no dye present in the polyethylene, delrin, and silicon substrates were mapped every 22 min until the bilayer broke, and the capacitance of the lipid films was measured before and after each scan. On the basis of these images, it was possible to measure the size of the tentatively assigned bilayer area, and $C_m$ values could be directly calculated through such correlations. A good statistical data set was created by analyzing data from 10 different bilayers for each substrate, and from each of these bilayers, more than 6 different images were examined. The capacitance versus area values are shown in Figure 5. For all three substrates, $C_m$ for most of the painted lipid films lies in the range of 0.3−1.0 $\mu$F/cm$^2$, indicating that our tentative assignment of the bilayer region is reasonable. A few SHG images, using delrin and polyethylene, revealed a highly uniform SHG signal inside the pore without any evidence of an annulus. This type of lipid film exhibited capacitance values of $<0.3$ $\mu$F/cm$^2$, indicating that only multilayer films were present.

Whereas the $C_m$ values for the three substrates were similar, there were some noticeable differences. Both types of plastic partitions exhibited multilayer formation (points below the lower limit in Figure 5a and b), but no multilayers were recorded using silicon. For the Si chips, we apparently formed two classes of BLMs. The first class was characterized by very thin bilayers

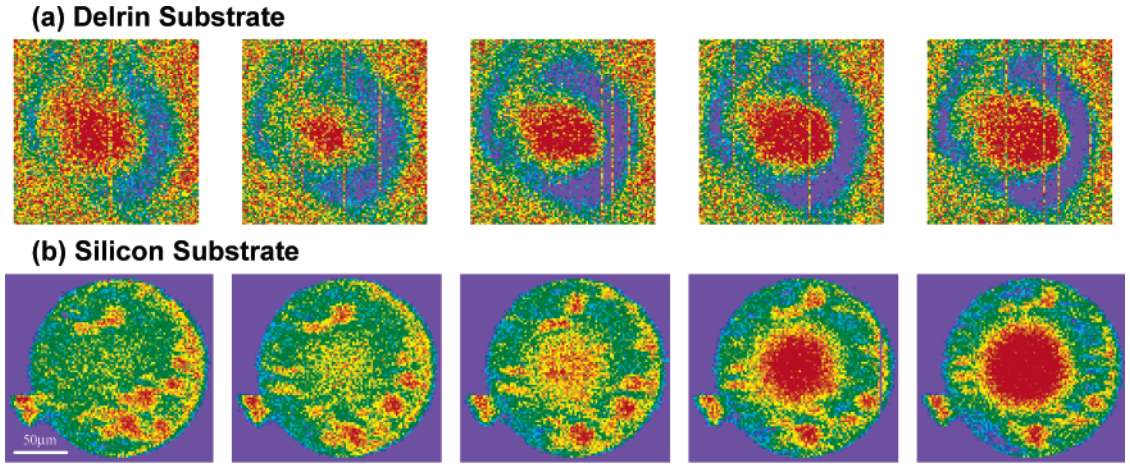


**Figure 6.** SHG images of bilayers suspended using (a) delrin and (b) silicon substrates and mapped at 22-min intervals.

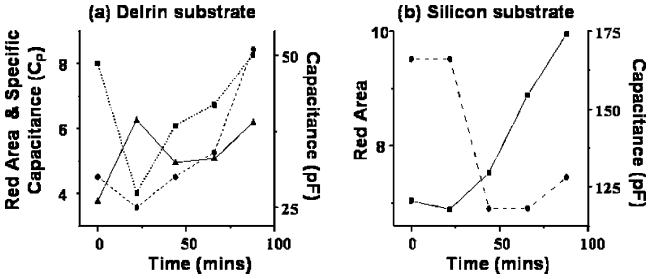


**Figure 7.** Time-dependent capacitance (●), $C_m$ (▲), and imaged bilayer area (■) change across the bilayer suspended in (a) delrin and (b) a silicon substrate. Units of $C_m$ and the red area are $\times 0.1$ $\mu$F/cm$^2$ and $\times 1000$ $\mu$m$^2$, respectively.

that had a capacitance around 200 pF or a $C_m$ near 1 $\mu$F/cm$^2$. The second class apparently had more incorporated decane and so was thicker, with a capacitance of around 100 pF or a $C_m$ in the range of 0.3−0.6 $\mu$F/cm$^2$. These silicon chip BLMs were very stable. An initial membrane capacitance value was measured directly after painting the bilayer. The capacitance value fluctuated around that initial value until the membrane broke. By comparison, the plastic partitions exhibited a large range of capacitance values, and during the lifetime of the bilayer, these values would often change, transitioning from a high to low capacitance and vice versa.

*3.2.3. Dynamics of Bilayer Formation.* The SHG microscopy experiments enabled us to follow the evolution of the BLM quantitatively over longer time periods, without the use of dye molecules, and as a function of the substrate. Whereas the gel phase of the SOPE lipids is sufficiently fluid to exhibit time-dependent dynamics, the painted bilayers are still somewhat ordered.[17] Thus, we expected to observe interesting structures in the system. SHG images of the suspended bilayer in the delrin and silicon substrates were taken every 22 min, and a sequentially taken subset of those images is shown in Figure 6, time sequenced from left to right. The full sequence of images can be seen in Supporting Information.

SHG images of the BLMs painted in the delrin substrate (Figure 6a) clearly show the time-dependent evolution of the bilayer structure. The first SHG image is of a freshly painted membrane, and the sequential ones reveal its time evolution. The red elliptical region is the bilayer, and this area can be extracted from each image and plotted along with the capacitance as a function of time (Figure 7a). Analyzing the data using the equations for $C_m$ reveals information about the bilayer thickness. On the basis of these values, there is an initial relaxation of the bilayer region to a smaller area and capacitance, followed by an expansion of the bilayer and an increase in capacitance. The bilayer slowly expanded at a rate of 61 ± 4 $\mu$m$^2$·min and had a small rise in capacitance of 0.37 ± 0.04 pF·min. An initial thinning of the bilayer occurs, followed by a period of constant thickness, and then a thinning once again until the bilayer broke. Temporal changes in bilayers were first noticed by White.[28] They observed bilayer formation for generally 30 min using a reflected-light imaging system and saw an almost constant $C_m$ that accompanied variations in the capacitance and area. Using a different delrin substrate, we also observed bilayers expanding and thinning simultaneously. In a series of scans, the capacitance increased by 0.28 ± 0.04 pF·min$^{-1}$, and the area increased by 25 ± 6 $\mu$m$^2$·min$^{-1}$. This correlated with an increase in $C_m$ at a rate of $1.6 \times 10^{-5}$ pF $\mu$m$^{-2}$·min$^{-1}$ as it changed from 0.54 to 0.82 $\mu$F·cm$^{-2}$ over 198 min. The slope associated with the $C_m$ is inversely proportional to the thickness, corresponding to a thinning of the bilayer. This thinning likely corresponds to decane being pushed out of the middle of the bilayer and into the annulus. This type of bilayer evolution is generally seen when voltages are applied.[10,28,29] The applied voltage changes the chemical potential of the annulus, forcing the bilayer to adjust the amount of incorporated solvent to maintain the free-energy minimum. If the bilayer cannot adjust the incorporated solvent to counterbalance the chemical potential change, then it will break. When we applied voltages to the bilayer in the delrin substrates, it usually led to the bilayers becoming leaky or breaking. We note that the manner in which this bilayer expands is contrary to the classical picture of the bilayer nucleating at the edge of the hole at the Plateau−Gibbs border (the bilayer/annulus interface) and then expanding, within a few minutes, in a zipperlike motion until a full BLM is present and a constant area achieved.[9,30]

BLMs suspended using silicon chips did not typically exhibit a significant change in $C_m$, but most bilayers exhibited an evolution of domain structures within the bilayer (i.e., the motion of microlenses and other regions of varying thickness). The SHG image series of Figure 6b and the corresponding plots of Figure 7b provide an interesting data set that reveals both the dynamics of domains within a bilayer and the power of SHG microscopy to resolve those domains. The series of images in Figure 6b reveals an increase in the red region that is characteristic of the thinnest portion of the bilayer; sequential images show the radial expansion of this region. As described above, the whole area imaged in Figure 6b was a bilayer with varying thicknesses, with the red region representing a very thin bilayer and the green and blue representing thicker regions as well as microlenses. Between the second and third frames of Figure 6b, a thinning

of the bilayer begins, and an extremely thin bilayer region starts to form. When the bilayer thins, most of the capacitance is now dropped over this smaller, thinner region, which causes the capacitance to drop rapidly to a lower value as seen in the dashed line of Figure 7b at $t = 44$ min. In Figure 7b, the change in area is plotted for the red region from these images, which was always increasing. The bilayer continued to expand, as measured both optically and electrically, because both the capacitance and the area of the red region increase. The bilayer capacitance was determined using the area of the image and the specific capacitance to prove that the red region is the main contribution to the capacitance. In the last image, the red region occupies about 35% of the bilayer region. We can correlate the measured area with the measured $C_m$ values in the following manner: by using $C_m$ values of 1.0 $\mu$F/cm$^2$ for the red region and 0.3 $\mu$F/cm$^2$ for the thicker portions, multiplied by the respective areas, we calculated a capacitance of 131 pF. This is close to the measured capacitance of 128 pF. This same analysis can be done for the other images in the sequence as well, reproducing the measured capacitances. These measurements demonstrate that SHG imaging is extremely sensitive to even small fluctuations in the thickness of the bilayer and that the bilayer thickness is a dynamic parameter.

## 4. Nonlinear Optical Imaging of BLMs Containing Field-Sensitive Dye Probes

**4.1. Overview.** In this section, we report on experiments in which molecular probes are utilized as additional tools to characterize the structure and dynamics of BLMs. As discussed above, SHG is a coherent scattering phenomenon generated by breaking the interface symmetry, and we demonstrated that SHG microscopy can distinguish between the different bilayer components. SHG imaging does not require but can be resonantly enhanced by fluorophores. By contrast, two-photon fluorescence (2PF) is an incoherent process involving photon absorption and emission that does depend on the presence of fluorescent molecules. Under appropriate conditions, both methods allow for the visualization of a suspended bilayer, and this has been previously demonstrated using lipid vesicles.[18] A further advantage of SHG imaging is that full polarization resolution of both the incident and collected radiation can yield molecular orientation information.[31−33] We utilize this to extract information relevant to the molecular probe orientation within the bilayer.

Certain membrane staining dyes have been synthesized that can provide interesting and complementary signatures for SHG and 2PF imaging. In particular, Loew and co-workers have developed special SHG dyes with large nonlinear coefficients.[34,35] Di-4-ANEPPS and di-8-ANEPPS were created to stain only one side of a bilayer leaflet and to exhibit a change in dipole moment when a potential across the membrane is varied. Because of this unique characteristic, these dyes have been used in place of voltage measurements (patch clamping) to determine membrane potential changes in cells.[19] At low concentrations, these dyes may be used to generate both SHG and 2PF imaging contrast. When these dyes are in solution, they are not SHG active because there is no broken interface symmetry. If the molecules are initially partitioned into just one side of the membrane and remain on that side, then the interface symmetry is broken, and a large SHG signal occurs. If the dye molecules were added to both sides of the bilayer where they equally partition into both sides, then there is no broken interface symmetry, which leads to no observable (resonant) SHG signal. Dye molecules that partition into lipid membranes are often capable of slowly switching (called flip-flop) from one leaflet of the bilayer to the other. If the dye molecules undergo flip-flop, then the symmetry of the system is slowly restored, and the SHG signal decreases. Because the dye molecules do not leave the bilayer but only undergo a rearrangement, the 2PF signal remains constant. Di-4-ANEPPS has a shorter acyl tail (by four carbon atoms) than di-8-ANEPPS, so only di-4-ANEPPS is expected to flip-flop. We validated this supposition by monitoring both dyes over long time periods.

These membrane potential dyes also provide additional evidence that the nonlinear microscope is capable of imaging specific components of the bilayer region. When the dye partitions into a bilayer and an electric field is applied, the dipole moment of the dye changes, and the SHG signal should change accordingly. If the dye is partitioned into a multilayer or some other stable state, there would be significantly less SHG signal enhancement due to the diminished electric field across the dye. Finally, we exploit polarization-resolved SHG imaging to determine some of the structural parameters and then develop a model of how di-8-ANEPPS resides in the membrane.

**4.2. Molecular Probe Incorporation into the Bilayer.** Separate methanol solutions (1 mg/mL of the di-4-ANEPPS and di-8-ANEPPS SHG probes) were prepared. A 2-$\mu$L aliquot of one of the solutions was dissolved in 1 mL of the buffer solution to be added to the bilayer. The dye was added to the top chamber, containing 3 mL of buffer, by a pipet, generally 50−200 $\mu$L at a time, and allowed to gravity diffuse into the pore. The bilayers were very stable, so the dye was allowed to partition into the bilayer for 15 min with no outside interference; then the chamber was rinsed and allowed to equilibrate for 30 min.

**4.3. Interaction between Dye Molecules and Lipid Bilayers.** The SHG-active and fluorescent dyes, di-4- and di-8-ANEPPS, having an electric-field-dependent $\chi^{(2)}$, were introduced into the bilayer as an additional structure and dynamics probe to complement the experiments described in section 3. Fluorophores are standard tools for visualizing and monitoring biological processes, so the interaction between fluorescent dyes and lipid membranes is an important issue.

Three aspects of dye molecules incorporated into a single-component suspended bilayer were characterized:

(1) Distribution of dye molecules into the lipid matrix.

(2) Interaction of the dipole moment of the dye with an electric field applied across the bilayer.

(3) Molecular orientation of the dye in the membrane.

All three of these should reflect the energetics of the surrounding lipid matrix. In addition, the field-dependent $\chi^{(2)}$ will also be dependent upon the alignment of the dye in the membrane and will be specific to each dye. When the dye is present, several different components of the resonance-enhanced SHG signal arise. Signal changes can arise from changes in the dye concentration due to bleaching or from changes in the dye orientation due to diffusion through the membrane. These components can be separated by simultaneously monitoring the BLM using 2PF. These dyes are often used in ratiometric studies, with only a small part of the emission curve being analyzed. By contrast, we integrated over the entire emission spectrum of the dyes, so we could utilize the 2PF signal as background normalization against the SHG signal.

*4.3.1. SHG Enhancement by SHG-Active Dyes.* The SHG-active dyes were first incorporated into the bilayer and monitored simultaneously with SHG and 2PF. Figure 8 shows a painted bilayer with and without a 50-$\mu$L aliquot of di-8-ANEPPS. When the plastic substrates were used, a large amount of scatter

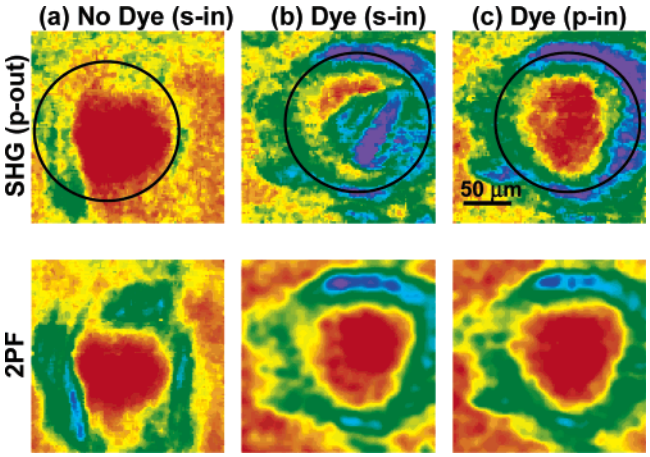


**Figure 8.** SHG and 2PF images of bilayers with and without the di-8-ANEPPS dye taken at $\lambda = 800$ nm in a polyethylene substrate. To clarify the area of the pore in the substrate, we depict the boundaries of the pore as black circles in the SHG images. The increased 2PF signal around the edge of the pore arises from increased scattering around the pore because the edges are not as smooth as the rest of the chip. Such a 2PF signal is not observed for the much smoother Si chips. Only the p-polarized SHG signal (p-out) was monitored, and the 2PF was an unpolarized signal. The SHG and 2PF images with dye were taken at two different polarizations of the fundamental light, s- (s-in), which increased 40 times compared to that in a, and p- (p-in), which increased 1.7 times compared to that in a, polarized light, and shown in b and c, respectively.

around the edges of the pore occurred. When these pores were processed rough edges around the top and bottom of the pore remained and acted as scattering centers and can therefore be seen in the 2PF images. When the dye was added, there was a corresponding 40-fold increase in the SHG intensity for s-in and a 2-fold increase in SHG intensity for p-in, but only a 1.3-fold increase in intensity for 2PF enhancement, which signifies that the dye incorporates into the bilayer. The di-8-ANEPPS was monitored for several hours, and the signal level did not change, implying that no flip-flop occurred, as was expected. If this experiment was repeated with the shorter di-4-ANEPPS (which has a shorter acyl chain), then the flip-flop should occur[36] and the SHG and 2PF signals should behave quite differently. When dye molecules reside on both sides of the bilayer the resulting symmetry should yield a smaller SHG signal because it relies on a noncentrosymmetric interface. However, flip-flop should not affect the 2PF intensity, so the 2PF signal can provide a normalization for the SHG data. Hence, a simultaneous measurement of both the SHG and 2PF intensities can yield a rate of flip-flop of a dye across the BLM. An excess of di-4-ANEPPS was added to the upper chamber of a freshly painted bilayer, and no dye was added to the lower chamber. SHG and 2PF images of bilayers were co-collected at an excitation wavelength of 850 nm. The SHG wavelength (425 nm) is close to the absorption maximum (470 nm). The di-4-ANEPPS signal was monitored for a long period of time, and the normalized signal intensity over time can be seen in Figure 9. We recorded a 122 ± 2 min half-life for the flip-flop of the dye molecule from the top leaflet to the bottom leaflet. This value was much longer than was observed for malachite green through a liposome.[17] This decreased rate of flip-flop in our experiment is most likely due to the lipids being in the tightly packed, gel phase of SOPE. It should also be noted that the small headgroup of phosphatidylethanolamine does not hinder the packing as do the headgroups in phosphaditylcholine or phosphatidylserine lipids,[17] leading to the SOPE being more densely packed.

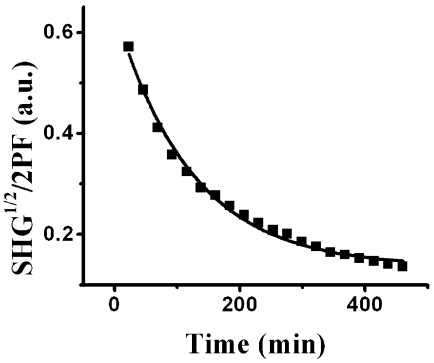


**Figure 9.** Flip-flop rate of di-4-ANEPPS through the bilayer was 122 ± 2 min. The filled squares are experimental data points, and the solid line is the fit.

*4.3.2. Voltage Dependence of the SHG Signal (Dipole Interaction).* The SHG-active dyes, with their field-dependent $\chi^{(2)}$ values, also yield additional evidence that we are truly interrogating a bilayer and not some other stable state of the lipids such as a liposome or multilayer. When these SHG-active dyes are incorporated into a membrane, the voltage applied to the membrane can be changed, and this will vary the SHG intensity. If the membrane is not a bilayer, then the electric field is decreased, and little or no voltage-dependent signal enhancement should occur. In these experiments, di-8-ANEPPS was incorporated into the suspended bilayer in the polyethylene substrate, and a change in the SHG intensity was monitored as the potential was varied across the lipid film. During the partitioning of the dye molecules into the system, images were collected to monitor the amount of signal enhancement. To not drastically change the composition of the bilayer, only a 100-$\mu$L aliquot of dye was added to the system, which has a total volume of 5 mL. To keep the dye concentration constant during the experiment, residual dye was removed by exchanging the solution in the upper chamber several times, and then the system was allowed to sit and equilibrate for 30 min.

The dye was added to two different lipid films, one with low specific capacitance ($<0.3$ $\mu$F/cm$^2$) and the other with high specific capacitance ($> 0.3$ $\mu$F/cm$^2$). In both systems, the SHG and 2PF signal increased once the dye partitioned into the bilayer. The applied voltage was varied between +100 and −100 mV during sequential scans, and only the high-capacitance film exhibited a voltage-dependent SHG response whereas the low-capacitance films showed no signal enhancement. In the absence of dye, no voltage-dependent SHG intensity was observed. The response was quantified by normalizing the SHG changes to the 2PF signal. An applied voltage of 100 mV led to a signal decrease by a factor of 0.62 ± 0.20, and −100 mV led to an enhancement by a factor 1.96 ± 0.20. The change in the SHG signal with applied voltage is expected to only occur in the bilayer because that is where the applied field is the largest. We interpreted these results as further quantitative evidence of the existence of a bilayer in the high-capacitance lipid films ($>0.3$ $\mu$F/cm$^2$).

*4.3.3. Orientation of the Dyes inside the Membrane.* SHG is a proven technique for measuring the molecular orientation on surfaces, but very little has been done with respect to applying this technique to bilayers. This presents a key opportunity to try to determine the molecular orientation of these dye molecules embedded within the bilayer. Because it does not undergo flip-flop, di-8-ANEPPS is the better candidate of our two dye molecules for a polarization-dependent study aimed at determining their orientation. Even though di-8-ANEPPS is not undergo-

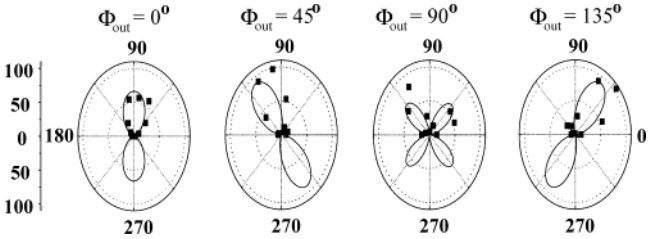


**Figure 10.** Representative polar plots, at various output polarizations, of the SHG signal vs the input polarization ($\Phi_{in}$) from di-8ANEPPS in a lipid bilayer suspended across a pore in a polyethylene substrate. The filled squares are experimental data, and the solid lines are the fits using eq 1. The input polarization is varied by 20° from 0 to 180°, and a scan is taken at each step. In these plots, p and s polarizations correspond, respectively, to 0 and 90°.

ing flip-flop, the lipid bilayer is still slowly moving, thus somewhat complicating the polarization-resolved measurements.

Figure 8 shows the SHG and 2PF signals co-collected ($\lambda$ excitation = 800 nm) from a BLM containing di-8-ANEPPS suspended across a polyethylene pore. In these images, significant 2PF and SHG signals were observed around the edges of the pore. The SHG signal arises from the interface symmetry being broken in the substrate at the edge of the pore. The increased 2PF signal arises from increased scattering around the pore because the edges are rough. In the 2PF images of Figure 8, there is only a small (1.3-fold) increase in 2PF inside the pore with the addition of dye, indicating a low concentration of dye in the bilayer. The SHG ($2\omega$) wavelength of 400 nm is far from the absorption peak (470 nm) of di-8-ANEPPS. Therefore, the two-photon excitation is only slightly resonant with the di-8-ANEPPS, which minimizes the 2PF increase. However, there is a huge difference in the SHG images with and without dye (Figure 8a and b). As shown in Figure 8b, the s-input polarization SHG image reveals stripelike domains (green and blue areas) inside the pore that are not observed without the dye. These domains are not observed with p-input polarization as seen in Figure 8c, suggesting at least some degree of orientation within these domains.

A full polarization data set for the SHG signal arising from these domains was collected to investigate the orientation of the dye molecules (Figure 10). Four output polarizations ($\Phi_{out}$) were used to monitor the SHG intensity as a function of input polarization ($\Phi_{in}$). Every stripelike domain seen in Figure 8 exhibited the same polarization characteristics, but the intensity levels from stripe to stripe were different. This suggests that the stripelike domains possess a slight concentration gradient of dye molecules across the bilayer that is picked up by the (off-resonant) SHG imaging because the intensity of the SHG signal is directly dependent upon the number of aligned dipoles in the excited volume. When all of the stripelike domains exhibit the same polarization dependence, this indicates that the dye is similarly aligned in each domain. This data and the concentration gradient that it implies indicate that the bilayer was chemically inhomogeneous.

The polarization of the SHG signal and its correlation to molecular orientation have been discussed in various reviews and papers.[27,31−33] The most common method for extracting the molecular orientation from the SHG data is based on the assumption that there are only one or two dominant molecular polarizability tensors in the molecules, such as $b_{ZZZ}$ or $b_{ZXX}$. Using these two molecular polarizability tensors, we tried to fit the data in Figure 10 assuming that the dye inside the bilayer might have a unique orientation. Under this assumption, the experimental data cannot be fit without using more than one

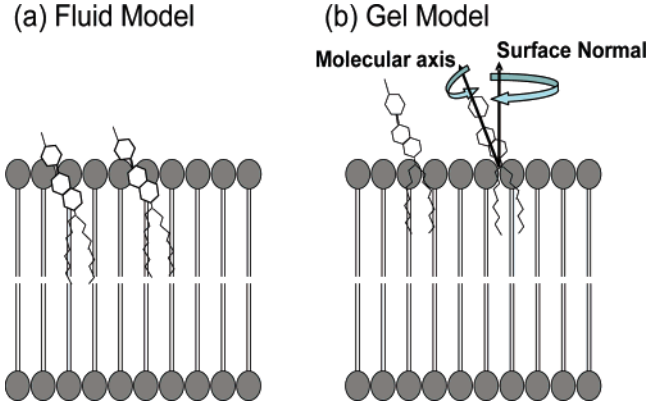


**Figure 11.** (a) Fluid model for the orientation of the dye molecule in the bilayer. In this model, the entire dye sits inside the bilayer region. (b) Gel-phase model suggested from the present experiments, in which the dye is anchored into the bilayer by its acyl chain. The molecular axis is tilted 36° to the surface normal, and the dyes freely rotate around both the surface normal and their molecular axis.

orientation. This then leads to the second assumption, which is that the molecules at the interface are randomly oriented in terms of rotation around the surface normal and the molecular axis. The equations to fit this data can be found in the Appendix along with an explanation of the fit. We looked at 10 different regions in the bilayer and determined that $\theta = 36 \pm 3°$, where $\theta$ is the tilt angle of the dye molecule from the surface normal. This value is similar to what was determined by Lambacher and Fromherz using fluorescence interferometry of dye-stained palmitoyl-oleoyl-phosphatidyl-choline lipids supported on a silicon chip rather than suspended across a pore, as was done here.[37] They calculated that di-8-ANEPPS was oriented 37.8 ± 1.6° from the surface normal.

Similar measurements were carried out to determine the orientation for di-4-ANEPPS. When using di-4-ANEPPS, we took images of bilayers at $l$ = 850 nm, of which the SHG wavelength (425 nm) is closer to the absorption peak (470 nm). With these two experimental variations, we observed a large increase in both the SHG and 2PF signals. With the addition of the dye molecules, the SHG signal from inside the pore greatly exceeded that observed from the silicon substrate. Generally, we observed larger SHG and 2PF signals when s-in polarization was used, and we collected a full complement of polarization data. This data was collected in about 50 min, or about half of the time it takes for the dye to undergo flip-flop. This data could not be fit using either of the assumptions used for the di-8-ANEPPS, suggesting that the lipid bilayer with di-4-ANEPPS is not isotropic around the surface normal. The di-4-ANEPPS does, of course, undergo the flip-flop process in the bilayer. This reduces the SHG signal intensity and may also obscure any orientation information in the polarization-dependent signal.

Upon the basis of the assumptions that were used to fit the experimental data and the rest of the information that we know about the dye and the BLM, we can develop a model for how the dye is oriented in the bilayer. Two different groups have previously looked at the orientation of this same class of dye molecules in bilayers made up of a mixture of phospholipids, but at higher temperatures (37 °C). The first group determined that the dye molecules should be embedded inside the bilayer[38] as shown in Figure 11a. The second group used a supported bilayer and determined that the dye was orientated at an angle of 37.8 ± 1.6° from the surface normal.[37]

Our system (a suspended SOPE bilayer at 25 °C in the gel phase) is much more constrained than the systems in either of

these two higher-temperature experiments, and this has structural implications. When we fit the data and found a molecular tilt angle of 36 ± 3° to the surface normal, we assumed that the dye molecules were either undergoing free rotation or were randomly distributed around the molecular axis and the surface normal. However, we can rule out the second possibility of random distribution because of the polarization dependence of the SHG signal in the collected SHG images. The domain structures we recorded in the images (Figure 8) imply that the dye molecules were not randomly orientated in the bilayer. Thus, the dye molecules must be freely rotating. Because there would be substantial steric hindrance for the dye molecules fully embedded in a bilayer, the di-8-ANEPPS molecules seem to be only partially partitioned into the bilayer; it is likely that they are anchored by having just their acyl chains embedded in the bilayer (Figure 11b).

Because fully embedded dye is observed in the less constrained (more fluid) bilayers, it may be that the rigidity of the bilayer dictates the extent of dye molecule penetration. Future experiments in which temperature and lipid compositions are varied should prove useful for testing this model.

## 5. Conclusions

We have reported here on the differences the supporting substrate introduces into the structure and the dynamics of the suspended bilayer; furthermore, we have attempted to quantify these differences.

Single-channel activity could be reconstituted into any bilayer, regardless of the substrate used. We faced clear advantages and disadvantages when utilizing each substrate material. Individual delrin and polyethylene are the easiest substrates to prepare and clean. Conversely, many identical silicon chips could be prepared using parallel device-processing techniques, and their surface properties were changed by the silanization of the silicon surface. The delrin and polyethylene substrates cannot be chemically modified to improve their hydrophobic character, which leads to greatly reduced bilayer stabilities. We found that the silicon-substrate-supported bilayers possess an immeasurable annulus but were decane-rich. A reasonable conclusion is that the decane decreases the tension of the annular region, thereby increasing the stability of the bilayer. However, the decane content of such a bilayer decreases over long time periods, eventually rendering the bilayer metastable. Silicon substrates also had a major disadvantage: we found that laser irradiation generates band gap excitations within the silicon chip and these interfered with the electrical measurements.

Nonlinear optical microscopy, coupled with an appropriate dye molecule and correlated with electrical measurements, has allowed us to quantify the structure and dynamics of suspended lipid bilayers at the molecular level. We observed and characterized various lipid−substrate and lipid−dye interactions. In particular, polarization-resolved SHG imaging yielded new information on the orientation of the dye molecules within the bilayer. Furthermore, the results highlight the importance of the structure of the dye and the phase behavior of the lipids to the membrane−dye interaction.

Suspended bilayers have become an important model system in the investigation of membrane biophysics. We have shown that the temporal evolution of the bilayers and the dependence of the morphology of the suspended bilayers on the substrate material are important factors in interpreting experimental measurements from these systems. Equally important, but not included in this study, is the influence of temperature because phenomena such as phase transitions and lipid raft formation will also contribute significantly to the behavior of the suspended bilayer systems. Thus, an investigation into the role of temperature in BLM systems at a similar level of analysis as that used in the present study should be useful, and we are carrying out pertinent experiments presently.

**Acknowledgment.** We acknowledge the W.M. Keck Foundation for assistance in constructing the SHG and 2PF microscopes used in this work. R.B. and F.B. acknowledge support from the National Institutes of Health (USPHS GM30376). J.R.H., R.S.R, and H.C. acknowledge the Institute for Collaborative Biotechnologies through grant DAAD19-03-D-0004 from the U.S. Army Research Office. We thank Dr. Leslie Loew for his helpful conversations and insight regarding the dyes.

## 6. Appendix

The SHG data in Figure 10 was fit under the assumptions that the dye was freely rotating around the surface normal and molecular axis; the polarization-dependent SHG signal is expressed as follows:[32]

$$I_{\mathrm{SHG}} \propto \left| \begin{aligned} &[(c_1\chi_{ZZZ} + c_2\chi_{ZXX} + c_3\chi_{XXZ})\cos^2\Phi_{in} + c_4\chi_{XXZ}\cos 2\Phi_{\mathrm{in}}]\cos\Phi_{\mathrm{out}} \\ &\qquad + c_5\chi_{ZXX}\sin^2\Phi_{\mathrm{in}}\sin\Phi_{\mathrm{out}} \end{aligned} \right|^2 I(\omega)^2 \tag{1}$$

$$c_1 = L_{ZZ}^{2\omega} L_{ZZ}^{\omega} L_{ZZ}^{\omega} \sin^2\theta_{\mathrm{in}} \sin\theta_{\mathrm{out}} \tag{2}$$

$$c_2 = L_{ZZ}^{2\omega} L_{XX}^{\omega} L_{XX}^{\omega} \cos^2\theta_{\mathrm{in}} \sin\theta_{\mathrm{out}} \tag{3}$$

$$c_3 = -L_{XX}^{2\omega} L_{XX}^{\omega} L_{ZZ}^{\omega} \sin 2\theta_{\mathrm{in}} \cos\theta_{\mathrm{out}} \tag{4}$$

$$c_4 = L_{YY}^{2\omega} L_{YY}^{\omega} L_{ZZ}^{\omega} \sin\theta_{\mathrm{in}} \tag{5}$$

$$c_5 = L_{ZZ}^{2\omega} L_{YY}^{\omega} L_{YY}^{\omega} \sin\theta_{\mathrm{out}} \tag{6}$$

where $\theta_{\mathrm{in}} = \theta_{\mathrm{out}} = 45°$ and $L_{ii}^{\omega}$ and $L_{ii}^{2\omega}$ correspond to Fresnel factors of the fundamental ($\omega$) and SHG ($2\omega$) light, respectively. In eq 1, there are only three independent second-order nonlinear susceptibility tensor elements, $\chi_{zzz}$, $\chi_{zxx}$, and $\chi_{xxz}$.

The SHG polarization plots were fitted using eq 1, and the fitted data is presented as solid lines in Figure 10. In this fit, the values of 1.0, −0.21, and 0.44 were used for $\chi_{zzz}$, $\chi_{zxx}$, and $\chi_{xxz}$. The fitted curves show reasonable agreement with the experimental data, except for a small offset (12°) of input polarization ($\Phi_{\mathrm{in}}$) angle. In our experimental setup, the flatness of the bilayer is questionable. Despite that, the SHG measurement was not disturbed because the focal depth (micrometer scale) is much longer than the thickness of the bilayer (nanometer scale). However, the polarization of light cannot be determined accurately, resulting in some slight uncertainty shown in Figure 10. Nonetheless, the general agreement between fitted data and experimental data indicates that the dye molecules are randomly oriented around a molecular axis and the surface normal.

We determined the tilt angle ($\theta$) of the molecular axis with respect to the surface normal, which can be expressed by the orientation parameter, $D$, as follows:[32]

$$D = \frac{\langle\cos^3\theta\rangle}{\langle\cos\theta\rangle} = \frac{\chi_{ZZZ} + \chi_{XXZ} - \chi_{ZXX}}{\chi_{ZZZ} + 3\chi_{XXZ} - \chi_{ZXX}} \tag{7}$$

For this experiment, we determined $D$ to be 0.65. If the dye molecules were evenly distributed with angle $\theta$ ranging between 0 and 90°, then $D$ would be 0.67, which closely corresponds to our result. However, the tail group of this dye is located in the bilayer, which makes the distribution of $\theta$ very narrow. If we assume that only one $\theta$ is possible, then the value of 0.65 correspond to $\theta = 36 \pm 3°$.

**Supporting Information Available:** Evolution of a suspended, single-component lipid bilayer viewed by second harmonic generation microscopy. This material is available free of charge via the Internet at http://pubs.acs.org.

## References and Notes


(1) Tien, H. T. *Bilayer Lipid Membranes: Theory and Practice*; Marcel Dekker: New York, 1974.

(2) White, S. H. The Physical Nature of Planar Bilayer Membranes. In Ion Channel Reconstitution; Miller, C., Ed.; Plenum Press: New York, 1985; p 3.

(3) Gennis, R. B. *Biomembranes: Molecular Structure and Function*; Springer-Verlag: New York, 1989.

(4) Hanke, W.; Schlue, W. R. *Planar Lipid Bilayers: Methods and Applications*; Academic Press Limited: San Diego, CA, 1993.

(5) *Lipid Bilayers: Structure and Interactions*; Katsaras, J.; Gutberlet, T.; Eds.; Springer-Verlag: New York, 2000.

(6) Mueller, P.; Rudin, D.; Tien, H. T.; Westcott, W. C. *Circulation* **1962**, *26*, 1167.

(7) Shalaev, E. Y.; Steponkus, P. L. *Biochim. Biophys. Acta* **1999**, *1419*, 229.

(8) Keller, S. L. *J. Phys.: Condens. Matter* **2002**, *14*, 4763.

(9) Tien, H. T. *J. Gen. Physiol* **1968**, *52*, 125s.

(10) Benz, R.; Janko, K. *Biochim. Biophys. Acta* **1976**, *455*, 721.

(11) Sintes, T.; Baumgartner, A.; Levine, Y. K. *J. Mol. Liq.* **2000**, *84*, 77.

(12) Forstner, M. B.; Kas, J.; Martin, D. *Langmuir* **2001**, *17*, 567.

(13) Ke, P. C.; Naumann, C. A. *Langmuir* **2001**, *17*, 5076.

(14) Starr, T. E.; Thompson, N. L. *Biophys. Chem.* **2002**, *97*, 29.

(15) Labarca, P.; LaTorre, R. *Methods Enzymol.* **1992**, *207*, 447.

(16) Eray, M.; Dogan, N. S.; Liu, L. J.; Koch, A. R.; Moffett, D. F.; Silber, M.; Vanwie, B. J. *Biosens. Bioelectron.* **1994**, *9*, 343.

(17) Srivastava, A.; Eisenthal, K. B. *Chem. Phys. Lett.* **1998**, *292*, 345.

(18) Moreaux, L., Sandre, O.; Mertz, J. *J. Opt. Soc. Am. B* **2000**, *17*, 1685.

(19) Bouevitch, O.; Lewis, A.; Pinevsky, I.; Wuskell, J. P.; Loew, L. M. *Biophys. J.* **1993**, *65*, 672.

(20) Campagnola, P. J.; Wei, M.; Lewis, A.; Loew, L. M. *Biophys. J.* **1999**, *77*, 3341.

(21) Lewis, A.; Khatchatouriants, A.; Treinin, M.; Chen, Z.; Peleg, G.; Friedman, N.; Bouevitch, O.; Rothman, Z.; Loew, L.; Sheres, M. *Chem. Phys.* **1999**, *245*, 133.

(22) Khatchatouriants, A.; Lewis, A.; Rothman, Z.; Loew, L. M.; Treinin, M. *Biophys. J.* **2000**, *79*, 2345.

(23) Wimmer, T.; Fucks, C.; Kryschi, C.; Martin, H. D.; Schmid, D. *J. Mol. Struct.* **2001**, *563*−*564*, 457.

(24) Bagatolli, L. A.; Gratton, E. *Biophys J.* **1999**, *77*, 2090.

(25) Bagatolli, L. A.; Gratton, E. *Biophys J.* **2000**, *78*, 290.

(26) Pantoja, R.; Sigg, D.; Bezanilla, F.; Heath, J. R. *Biophys. J.* **2001**, *81*, 2389.

(27) Choi, H.; Yang, X.; Mitchell, G. W.; Collier, C. P.; Wudl, F.; Heath, J. R. *J. Phys. Chem. B* **2002**, *106*, 1833.

(28) White, S. H.; Thompson, T. E. *Biochim. Biophys. Acta* **1973**, *323*, 7.

(29) Rosen, D.; Sutton, A. M. *Biochim. Biophys. Acta* **1968**, *163*, 226.

(30) Tien, H. T. *J. Theor. Biol.* **1967**, *16*, 97.

(31) Shen, Y. R. *Annu. Rev. Phys. Chem.* **1989**, *40*, 327.

(32) Corn, R. M.; Higgins, D. A. *Chem. Rev.* **1994**, *94*, 107.

(33) Eisenthal, K. B. *Chem. Rev.* **1996**, *96*, 1343.

(34) Loew, L. M.; Simpson, L. L. *Biophys. J.* **1981**, *34*, 353.

(35) Huang, Y. W.; Lewis, A.; Loew, L. M. *Biophys. J.* **1988**, *53*, 665.

(36) Loew, L. M.; Cohen, L. B.; Dix, J.; Fluhler, E. N.; Montana, V.; Salama, G.; Wu, J. Y. *J. Membr. Biol.* **1992**, *130*, 1.

(37) Lambacher, A.; Fromherz, P. *J Phys. Chem. B* **2001**, *105*, 343.

(38) Gross, E., Bedlack, R. S.; Loew L. M. *Biophys. J.* **1994**, *67*, 208.